Hyperfine structure, optical dephasing, and spectral-hole lifetime of single-crystalline $Pr^{3+}:La_2(WO_4)_3$

O. Guillot-Noël,* Ph. Goldner, Y. Le Du, and P. Loiseau
Laboratoire de Chimie de la Matière Condensée de Paris, Ecole Nationale Supérieure de Chimie de Paris (ENSCP), CNRS-UMR 7574, ENSCP, 11 rue Pierre et Marie Curie 75231 Paris Cedex 05, France

B. Julsgaard, L. Rippe, and S. Kröll
Department of Physics, Lund Institute of Technology, P.O. Box 118, S-22100 Lund, Sweden
(Received 8 January 2007; published 15 May 2007)

Most of the experiments related to quantum information applications, involving rare-earth doped inorganic crystals, are performed on yttrium orthosilicate single crystals. The work presented here is motivated by the search of new compounds which can be used in the field of quantum computing and/or quantum storage. Relaxation times and hyperfine structure of the $^3H_4(0)\rightarrow{}^1D_2(0)$ transition in 1.4% $Pr^{3+}:La_2(WO_4)_3$ at 4 K have been measured by photon-echo and spectral-hole-burning techniques. The hyperfine splittings of the ground $^3H_4(0)$ and the excited $^1D_2(0)$ states are 14.9±0.1 MHz, 24.6±0.1 MHz and 5.0±0.1 MHz, 7.3±0.1 MHz, respectively. An inhomogeneous linewidth of 18.8±0.1 GHz was measured. A homogeneous linewidth of 25.3±2.0 kHz was obtained with or without an external magnetic field of about 14 mT. The fluorescence dynamics of the $^1D_2$ level obtained by a direct excitation in the $^3H_4\rightarrow{}^1D_2$ transition gives a nonexponential decay which indicates energy-transfer processes. This decay can be accurately fitted by the Inokuti-Hirayama model [J. Chem. Phys. **43**, 1978 (1965)] with a radiative lifetime of 61±1 μs giving a minimal homogeneous linewidth of 2.6 kHz. The spectral-hole lifetime due to population redistribution within the ground hyperfine levels is 16±2 s. The results obtained for the $La_2(WO_4)_3$ compound make this crystal an interesting host for quantum applications.

DOI: 10.1103/PhysRevB.75.205110 PACS number(s): 78.55.−m, 42.50.Md, 42.62.Fi

I. INTRODUCTION

Rare-earth ions in inorganic crystals (REICs) are promising candidates in the quest for macroscopic quantum effects and, in particular, in the areas of quantum computing (QC) (Refs. 1 and 2) and quantum state storage (QS) (Refs. 3 and 4). Indeed, some rare-earth ions possess long-lived nuclear-spin ground-state levels (hyperfine levels), well isolated from the environment. These levels can be put into a coherent superposition for a long time and can potentially be used for storage of quantum and classical information. At low temperature (1.5 K), a hyperfine coherence (T_2) lifetime >1 s has been reported in $Pr^{3+}:Y_2SiO_5$.[5] Moreover, rare-earth optical transitions can also exhibit a long coherence lifetime (up to 6.4 ms).[6]

In the field of QS, two different schemes have been proposed[7–10] and storage has been demonstrated for classical and quantum light essentially in atomic vapor.[11–14] One of the schemes is based on the phenomena of electromagnetically induced transparency (EIT) and slow light.[11] EIT, slow, and stopped light have been demonstrated in REIC. For example, in $Pr^{3+}:Y_2SiO_5$, light was stopped during times greater than 1 s.[3] Another scheme is based on methods of pulse-shape storage using photon echoes.[4,9,15] Moiseev and Kröll have described a scheme for reconstructing the quantum state of a nonstationary single-photon wave packet absorbed in a macroscopic medium with a Doppler-broadened transition.[9] This scheme exploits the fact that frequency shifts due to Doppler effect are opposite for counterpropagating fields. As rare-earth ions are commonly used to perform coherent spectroscopy experiments, such as hole burning and photon echoes,[6] this idea has been extended to REIC.[4] In the solid-state case, the absence of Doppler broadening necessitates the creation of a reversible artificial inhomogeneous broadening which can be obtained by applying a reversible inhomogeneous external electric field that shifts the resonance frequencies of ions in different positions in the medium by means of the Stark effect. The first demonstration of such scheme was reported by Alexander *et al.*[16] A photon echo was obtained in $Eu^{3+}:Y_2SiO_5$ by producing a reversible inhomogeneous broadening of the Eu^{3+} $^7F_0\rightarrow{}^5D_0$ optical transition with an external electric field gradient.

For the photon-echo approach, a two-level system is sufficient for the quantum state storage, but for storage in the excess of the quantum state coherence time, a three-level Λ system is required for both the EIT and photon-echo schemes. A three-level Λ system consists of two levels, which can both be coupled by light fields to a higher third one. The field to be stored is resonant with one of the transitions and a second driving field with the other one.

In order to achieve an efficient QS with REIC, the system has to fulfill several criteria which are common to both schemes.[17] Firstly, the coherence time T_2 of the transition has to be long and it should preferably be limited by the oscillator strengths to the lower transitions. Several dominant mechanisms contribute to the homogeneous linewidth of rare-earth ions: (i) the broadening due to the natural lifetime of the excited state, (ii) the rare-earth–rare-earth interactions, (iii) the rare-earth–host interaction mainly due to nuclear and electron-spin fluctuations of the host lattice, and (iv) the coupling to phonons.[18] The first contribution can be reduced by working with rare-earth ions having long radiative lifetime.

The second contribution is directly linked to the rare-earth concentration; low doping level should therefore be used. The third contribution could be reduced by using materials with low nuclear-spin density.[19] An additional external magnetic field can be used to freeze the spin fluctuations.[18] The fourth contribution is strongly suppressed at 4 K. Secondly, active material must completely absorb the wave packet. For REIC, this means that the absorption depth must be high, i.e., $\alpha L \gg 1$, when the transition is broadened by the electric field, where α is the absorption coefficient and L is the total length of the absorbing medium. In order to realize a Λ system, the hyperfine levels of the rare-earth ion can be used, and optical transitions connecting two ground-state hyperfine levels with a common excited-state level must be allowed. This requires that the nuclear-spin states are mixed in the energy eigenstates of the hyperfine levels, since optical transitions are limited by the nuclear-spin projection selection rule, $\Delta M_I = 0$. This mixing can be obtained by using hosts with low site symmetry for the rare-earth ions and/or applying an external magnetic field with a particular orientation.[20–22] When rare-earth ions are doped at random into an inorganic crystal, each ion is located in a slightly different local environment in the host, giving an inhomogeneous broadening of the optical transition. To preserve a large αL value, the inhomogeneous linewidth should be reduced in order to have enough absorbing ions per homogeneous frequency channel. Thirdly, in order to be able to optically drive the ions participating in the storage, without exciting the ions that are not participating, materials where the hyperfine splitting is larger than the optical linewidth must be used.

In the field of QC science, some schemes using rare-earth ions for the implementation of quantum computing were proposed.[1,2] In the latter, the quantum information is also stored in two rare-earth ground-state hyperfine levels that constitute the qubit states. Different qubits are defined in the frequency domain, which is made possible by the inhomogeneous broadening. Qubit operations are performed using highly stabilized lasers driving homogeneous channels in the optical transitions. The large ratio between the inhomogeneous linewidth and the homogeneous linewidth (around 10^7 for rare-earth ions) provides a very large number of individually addressable qubits. Logical quantum gates are achieved by using interactions between rare-earth ions due to electric dipole-dipole coupling. Nilsson *et al.* and Rippe *et al.* demonstrated the first steps of viability of quantum information processing with REIC in $Pr^{3+}:Y_2SiO_5$.[23–25] Longdell *et al.* realized a conditional quantum phase shift between two europium ions in Y_2SiO_5.[26] For quantum computing application, the REIC has to fulfill similar criteria as in the QS area. Ion-ion coupling through electrostatic interaction is an additional criterion to consider for the realization of controlled logic gates. Hosts where rare-earth ions have a permanent electric dipole moment are thus required.

Most of the experiments involving REIC for quantum applications have so far been performed on yttrium orthosilicate single crystals. The work presented here is motivated by the search of new compounds, which can fulfill the previous criteria, and which are not all fulfilled in YSO. We decided to work on $Pr^{3+}:La_2(WO_4)_3$ single crystals for several reasons.

(1) Pr^{3+} ions have sharp optical resonances with long optical coherence times. Pr^{3+} ions present a hyperfine structure at zero magnetic field due to the 100% abundant ^{141}Pr isotope with a nuclear spin $I=5/2$. Pr^{3+} ions can be driven by stabilized dye laser on the lowest crystal-field states of the $^3H_4 \rightarrow {}^1D_2$ transition around 602.76 nm in $La_2(WO_4)_3$. Pr^{3+} ions have high transition strengths and present strong electrostatic dipole coupling. Pr^{3+} hyperfine splittings are generally higher than the homogeneous linewidth of the transition.

(2) Tungstate hosts are interesting because tungsten has only one stable isotope (^{183}W) with a nonzero magnetic moment (0.12 nuclear magneton) and it has a natural abundance of 14.3%. This is favorable for low homogeneous linewidth as spin fluctuations in the surroundings of the rare earth decrease the dephasing time of the transition.

(3) In $La_2(WO_4)_3$, Pr^{3+} ions substitute La^{3+} ions. As these ions have nearly the same ionic radius, $r_{La}=1.18$ and $r_{Pr}=1.14$,[27] substitution of La^{3+} by Pr^{3+} will not induce large strains in the crystal and one can expect to obtain low inhomogeneous linewidth. On the negative side, La^{3+} ions present a high nuclear moment (^{139}La, abundance 99.91% with a nuclear magnetic moment of 2.78 in nuclear magnetons) which can cause an important contribution to the homogeneous linewidth through spin-flip fluctuations. Taking into account crystal structures and nuclei magnetic moments, the magnetic moment density in $La_2(WO_4)_3$ is 2.19×10^{22} nuclear magnetons/cm^3 compared to 2.87×10^{21} nuclear magnetons/cm^3 in Y_2SiO_5. Lanthanum based compounds are thus a compromise between low inhomogeneous linewidth and high rare-earth–host interactions.

(4) Lanthanum tungstate crystal $La_2(WO_4)_3$ belongs to the monoclinic system with space group $C2/c$.[29] Pr^{3+} ions substitute La^{3+} ions in only one crystallographic site of C_1 symmetry. In low site symmetry, the nuclear-spin projection is mixed, which is favorable for high transition strengths. Moreover, the absence of a symmetry center allows the rare-earth ions to have a permanent electrostatic dipole.

In this work, by using photon-echo and hole-burning techniques, we have determined the hyperfine structure, the optical dephasing, the inhomogeneous linewidth, and the spectral-hole lifetime of single-crystalline 1.4% $Pr^{3+}:La_2(WO_4)_3$. The paper is organized as follows. In Sec. II, we present the experimental apparatus. In Sec. III, the experimental results are presented and discussed.

II. EXPERIMENT

$Pr^{3+}:La_2(WO_4)_3$ single crystals were grown by the Czochralski method following the procedure explained in Ref. 28. Lanthanum tungstate crystal belongs to the monoclinic system with space group $C2/c$, with unit parameters $a=7.873(2)$ Å, $b=11.841(2)$ Å, $c=11.654(2)$ Å, $\beta=109.25(3)$, and $Z=4$.[29] Pr^{3+} ions substitute La^{3+} ions in only one crystallographic site of C_1 symmetry. The Pr concentration determined by inductively coupled plasma atomic spectroscopy is $1.4\% \pm 0.2\%$ which corresponds to 1.09 ± 0.1510^{20} at./cm^3.

The measurements were performed on the transition between the lowest crystal-field levels of the $^3H_4$ and $^1D_2$ multiplets at 602.76 nm (in vacuum) in $La_2(WO_4)_3$. The sample

is a plate of 3×6 mm^2 with a thickness of 1.33 mm in the direction of light propagation. The sample was immersed in liquid helium at a temperature of 4 K. A Coherent CR-699-21 ring dye laser, pumped by a Spectra Physics 2080 argon-ion laser, operating with Rhodamine 6G, provided the correct wavelength resonant with the $^3H_4(0)\rightarrow{}^1D_2(0)$ transition. The cw dye laser is linearly polarized and operates in a single servo-locked mode with a spectral width of 1 MHz. The wavelength was determined by a homemade Michelson-type wavemeter.

In the photon-echo measurement, the light was gated by two ISOMET 1205C acousto-optic modulators (AOMs), controlled by ISOMET D322B drivers creating excitation pulses with a duration in the range 500–1000 ns at a repetition rate of 10 Hz. A modulator with a bandwidth of 40 MHz was used in a double-pass configuration in order to increase the bandwidth (80 MHz) and to eliminate beam movement accompanying the frequency shifts. The light pulses were focused on the crystal to a measured beam diameter of around 100 μm. A third acousto-optic modulator was put after the cryostat to gate the detection, blocking the transmitted excitation pulses. The echo signal was detected by a photomultiplier tube (Hamamatsu R943-02) and recorded by a Tektronx 2431 L oscilloscope. The reference beam was detected using a homebuilt amplified photodiode. The laser was continuously scanned over 1 GHz for 2.5 s in order to avoid hole-burning effects during the photon-echo measurements. The pulse sequences were computer controlled and the echo intensities averaged over 256 scans. The photon echo was measured at the peak of the absorption line. The energy of the laser was measured by a Coherent Fieldmaster LM-2 power meter. Excitation intensities between 3 and 80 W/cm^2 were used. The laser intensity I was calculated from the power P as $2P/(\pi w^2)$, where w is the Gaussian beam radius where the intensity has decreased to $1/e^2$. A static field of about 14 mT, provided by a pair of Helmholtz coils, could be applied perpendicular to the light propagation in the crystal in order to study how a magnetic field influences the homogeneous linewidth.

In the hole-burning experiment, the readout of spectral features after burning was performed by scanning the light frequency and recording the intensities of the transmitted and reference beams using a matched pair of electronically amplified photodiodes. The burning pulse was 1 ms long. During the probing pulse, the laser was scanned over 80 MHz for 600 μs with the intensity reduced by 2–3 orders of magnitude relative to the burning pulse. The separation between the burning and reading pulse is 100 μs and recording is done in a single shot in order to avoid laser-frequency jitter which will decrease the resolution of the hole-burning spectrum. The AOMs were driven by a 1GS/s Tektronix AWG520 arbitrary wave-form generator, which allowed direct control of pulse amplitude and phase and which ensured a precise scan of the frequency. The transmission hole-burning spectrum and the reference signal were recorded by a Tektronix TDS 540 oscilloscope and transferred to a computer.

The spectral-hole lifetime was measured by burning a hole in the absorption line and then probing the spectral hole after a variable time in the range 0–25 s.

The lifetime of the excited $^1D_2$ CF level was recorded using a Jobyn-Yvon H25 spectrometer and a Princeton Instruments intensified charge coupled device camera. Pulsed excitation (8 ns duration) was provided by a BMI optical parametric oscillator pumped by the third harmonic of BMI Nd doped yttrium aluminum garnet laser. The fluorescence intensity at 606.76 nm was recorded as function of time, 25 ns after the laser pulse and for 500 μs.

III. RESULTS AND DISCUSSION

A. Hyperfine structure

The hyperfine structure of the $^3H_4(0)$ ground state and of the $^1D_2(0)$ excited state is obtained in the frequency domain by spectral-hole burning. Pr has one 100% abundant isotope (^{141}Pr) with a nuclear spin $I=5/2$. In a low site symmetry, the electronic degeneracy of the $^3H_4$ and $^1D_2$ multiplets is totally lifted, giving rise to electronic singlets. As the orbital angular momentum is quenched, the hyperfine interaction is zero to first order. At zero magnetic field, the hyperfine splittings are due to a "pseudoquadrupole interaction" which is the combination of the second-order hyperfine interaction and of the pure nuclear quadrupole interaction. In a particular hyperfine manifold, at zero magnetic field, the following effective spin Hamiltonian can be used to describe the hyperfine splittings:[30]

$$H=\mathbf{I}\cdot(A_J^2\mathbf{\Lambda}+\mathbf{P})\cdot\mathbf{I}, \tag{1}$$

where $\mathbf{I}$ is the nuclear spin, $\mathbf{P}$ is the pure quadrupole tensor, and the $\mathbf{\Lambda}$ tensor is given by

$$\Lambda_{\alpha\beta}=\sum_{n=1}^{2J+1}\frac{\langle 0|J_\alpha|n\rangle\langle n|J_\beta|0\rangle}{E_n-E_0}. \tag{2}$$

The index 0 denotes the first crystal-field singlet level of the $^3H_4$ and $^1D_2$ multiplets, n is the other crystal-field levels, and E_n is the energy of the crystal-field level. α and β stand for x, y, z. A_J is the hyperfine constant of the J multiplet. In low site symmetry, the principal axes of the $\mathbf{P}$ and $\mathbf{\Lambda}$ tensors are not coincident. However, we can define a third set of principal axes (x'',y'',z'') which gives the following form for the effective Hamiltonian:[18]

$$H'=D[I_{z''}^2-I(I+1)/3]+E(I_{x''}^2-I_{y''}^2). \tag{3}$$

Each crystal-field level of a J multiplet is characterized by a set of D and E values and by its own principal axes.[31] This Hamiltonian splits the $^3H_4(0)$ and $^1D_2(0)$ into three doubly degenerate hyperfine levels. As the hyperfine splittings are smaller than the inhomogeneous broadening, each allowed transition between the hyperfine levels of the ground and excited states will be resonant with the frequency of the burning laser for some subset of ions. If all the transitions are allowed, a pattern of three side holes and 21 antiholes is thus expected on each side of the central primary hole. The frequency intervals between the primary hole and side holes give the hyperfine splittings of the excited $^1D_2(0)$ state, whereas the frequency intervals between the primary hole and antiholes give the hyperfine splittings of the $^3H_4(0)$ ground state, as well as the sum and difference of the excited- and ground-state splittings. Figure 1 displays the

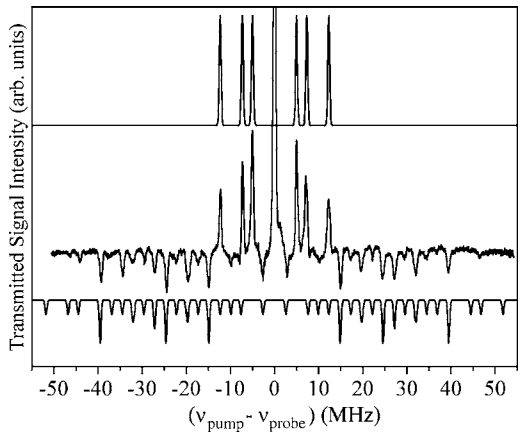

FIG. 1. Transmission hole spectrum at 4 K for the transition between the lowest crystal-field level of the $^3H_4$ and $^1D_2$ multiplets. The upper (lower) diagram shows the hole (antihole) pattern.

transmission hole spectrum for the $^3H_4(0) \rightarrow {}^1D_2(0)$ transition and the simulated hole and antihole pattern. For the simulation, only the positions of the lines were fitted. For the intensities, we considered that each transition within the hyperfine structure has the same transition strength. A resonant hole width of about 1 MHz, limited by laser-frequency jitter and readout chirp rate, was achieved. The hyperfine splittings of the ground and excited states are given in Table I. From the hyperfine splittings and Eq. (3), the spin-Hamiltonian parameters D and E are calculated for the ground and excited states. As it is not possible from hole-burning experiments only to determine the order of the hyperfine splittings for both states, the signs of D and E cannot be specified. The Hamiltonian H' was diagonalized and the hyperfine constants were fitted by comparing the calculated splittings with the experimental ones. The E term in Eq. (3) is responsible for the M_I mixing. The E values in $La_2(WO_4)_3$ are comparable to the ones measured in Y_2SiO_5 (Ref. 31): $D=4.44$ MHz, $E=0.56$ MHz for $^3H_4(0)$ and $D=1.36$ MHz, $E=0.42$ MHz for $^1D_2(0)$. We can thus expect as in Y_2SiO_5 a mixing of the nuclear-spin projections in $La_2(WO_4)_3$, causing the $\Delta M_I=0$ selection rule to break down for optical transitions.

B. Inhomogeneous and homogeneous linewidths

The inhomogeneous linewidth (Fig. 2) of the $^3H_4(0) \rightarrow {}^1D_2(0)$ transition of 1.4% Pr^{3+}:$La_2(WO_4)_3$, measured with the cw dye laser by monitoring the transmitted intensity while scanning the laser over 100 GHz, is 18.8±0.1 GHz (full width at half maximum). For a 0.1% doped Y_2SiO_5 single crystal, which corresponds to 1.6×10^{19} at./cm^3,[3] if we assume that 90% of the ions occupy site 1, the inhomogeneous linewidth of the same transition for Pr^{3+} ions in site 1 is 30 GHz (Ref. 32) and for a 0.02% doped crystal it is 4.4 GHz (Ref. 33). In Eu doped Y_2SiO_5, the inhomogeneous linewidth has been shown to scale approximatively linearly with the concentration.[34] Site 1 in Y_2SiO_5 is the site of interest for quantum state manipulation. For the lanthanum compound with a ten times higher doping level, we already have a lower inhomogeneous linewidth. This behavior confirms that substituting La^{3+} ions instead of Y^{3+} ions by Pr^{3+} ions can reduce the crystal strains due to the dopant. We can thus expect to have a lower inhomogeneous linewidth in the lanthanum compound than in the silicate compound at equivalent concentration. From the spectrum of Fig. 2, an absorption coefficient $\alpha=14.7$ cm^{-1} is measured, which gives a peak absorption cross section $\sigma_a=1.35\times10^{-19}$ cm^2 and an oscillator strength of 2.3×10^{-8}. The oscillator strength of Pr^{3+} in $La_2(WO_4)_3$ is lower than that of site 1 (3×10^{-7}) in Y_2SiO_5.[33]

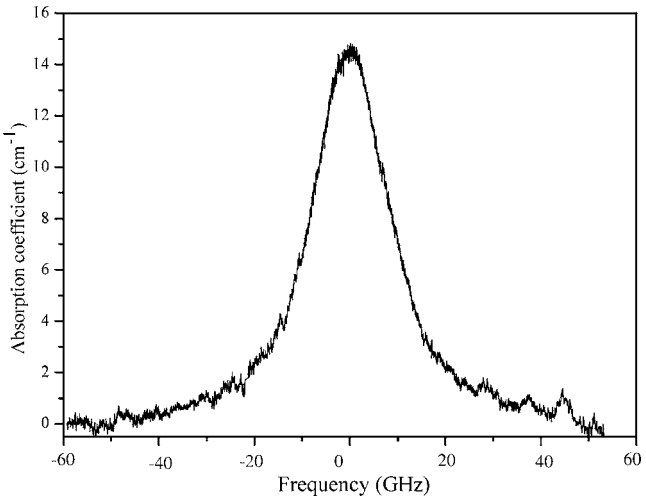

FIG. 2. Absorption coefficient versus frequency for the $^3H_4(0) \rightarrow {}^1D_2(0)$ transition in 1.4% Pr^{3+}:$La_2(WO_4)_3$.

TABLE I. Hyperfine splittings of the $^3H_4(0)$ and $^1D_2(0)$ states. The spin-Hamiltonian parameters are also given.

Frequency (MHz)	$^3H_4(0)$	$^1D_2(0)$
δ_1	14.9±0.1	5.0±0.1
δ_2	24.6±0.1	7.3±0.1
$\delta_1+\delta_2$	39.7±0.2	12.3±0.2
$\lvert D\rvert$	6.35±0.05	1.92±0.05
$\lvert E\rvert$	0.88±0.05	0.36±0.05

As discussed in the Introduction, homogeneous linewidth Γ_h of the $^3H_4(0) \rightarrow {}^1D_2(0)$ transition was determined by using two-pulse photon-echoes. The photon-echo signals decay, as a function of separation t_{12} between pulses, as $\exp(-4t_{12}/T_2)$ where T_2 is related to Γ_h by $\Gamma_h=\frac{1}{\pi T_2}$. Figure 3 gathers the two-pulse photon-echo decays as function of t_{12} for the $^3H_4(0) \rightarrow {}^1D_2(0)$ transition measured in 1.4% Pr^{3+}:$La_2(WO_4)_3$ at 4 K with an excitation intensity of around 8 W/cm^2. The optical dephasing time $T_2=11.2\pm0.6$ μs yields a homogeneous linewidth $\Gamma_h=28.4\pm2.0$ kHz.

The homogeneous linewidth Γ_h can be written as a sum of contributions from several mechanisms:[18]

$$\Gamma_h = \Gamma_{\text{pop}} + \Gamma_{\text{ion-ion}} + \Gamma_{\text{ion-spin}} + \Gamma_{\text{phonon}}, \quad (4)$$

where Γ_{pop} is the contribution from the excited-state population lifetime, $\Gamma_{\text{ion-ion}}$ is the contribution from changes in the

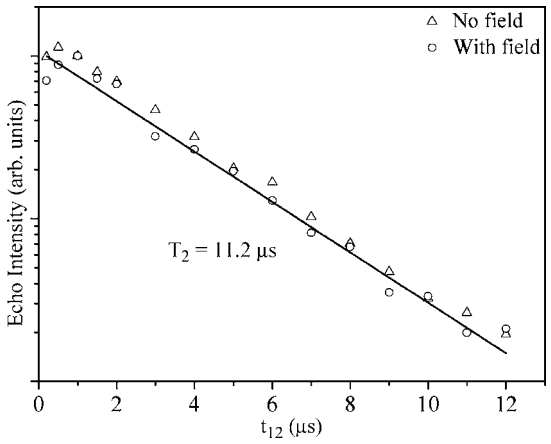

FIG. 3. Two-pulse photon-echo decays of the $^3H_4(0) \rightarrow {}^1D_2(0)$ transition measured in 1.4% Pr^{3+}:$La_2(WO_4)_3$ at 4 K with and without a magnetic field of 14 mT. The excitation intensity is around 8 W/cm^2. The fit that assumes an exponential decay is represented by a straight line.

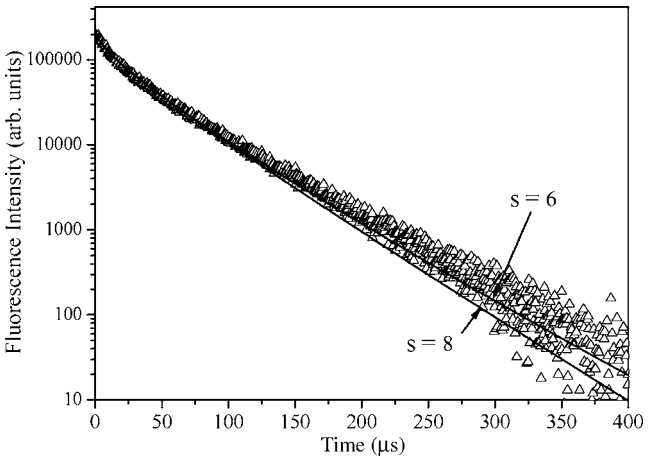

FIG. 4. Fluorescence decay of the $^3H_4 \rightarrow {}^1D_2$ transition in 1.4% Pr^{3+}:$La_2(WO_4)_3$ at 12 K. The solid lines are obtained by using the Inokuti-Hirayama model with $s=6$ and $s=8$ corresponding to dipole-dipole and dipole-quadrupole interactions, respectively. The best fit is obtained with $s=6$.

local environment due to the optical excitation or population relaxation of other ions, the so-called instantaneous spectral diffusion, $\Gamma_{\text{ion-spin}}$ is the contribution due to nuclear- and electron-spin fluctuations of the host lattice, and Γ_{phonon} includes contributions from temperature dependent phonon scattering. At 4 K, Γ_{phonon} is frozen out so this contribution is negligible in our work.

The first term Γ_{pop} contains contribution from radiative and nonradiative decay (T_1) and gives the ultimate limit on Γ_h. There is a large energy gap below the $^1D_2(0)$ excited state, which implies that contribution to Γ_{pop} from spontaneous phonon emission is very small. The fluorescence dynamics of the $^1D_2$ level was obtained by a direct excitation in the $^3H_4 \rightarrow {}^1D_2$ transition at 12 K (Fig. 4). A nonexponential decay is observed which indicates energy-transfer processes. At short times, the decay is fast and dominated by energy transfers between close lying ions. At longer times, transfers between ions separated by larger distances and spontaneous relaxation are more important so that the fluorescence decays at a lower rate.

Several models have been proposed to explain nonexponential decay: (i) diffusion process where the excitation moves from donor to donor before being transferred to an acceptor or a trap and (ii) direct transfer between one acceptor and one donor without diffusion.[35] The model that we propose in 1.4% Pr^{3+}:$La_2(WO_4)_3$ is a direct resonant cross-relaxation mechanism, without diffusion, involving two identical Pr^{3+} ions (donor and acceptor) according to the following scheme: $[{}^1D_2, {}^3H_4] \rightarrow [{}^1G_4, {}^3F_4]$. This kind of relaxation has already been observed in several Pr doped systems as, for example, in $LiNbO_3$,[36] in fluorapatite crystals,[37] in yttria-stabilized zirconia,[38] and in $LiKYF_4$ crystal.[39] The decay curve in Fig. 4 can be accurately fitted by the Inokuti-Hirayama model:[40]

$$I(t) = I(0)\exp\left[-\frac{t}{\tau_r} - \Gamma\left(1-\frac{3}{s}\right)\frac{N}{C_0}\left(\frac{t}{\tau_r}\right)^{3/s}\right], \qquad (5)$$

where τ_r is the radiative lifetime, N is the concentration of the luminescent centers, $C_0 = \frac{3}{4\pi R_0^3}$ is the critical concentration, and R_0 is the critical radius defined as the distance at which an isolated donor-acceptor pair has the same transfer rate as the spontaneous decay rate of the donor. The s parameter is equal to 6, 8, or 10 with an electric dipole-dipole, dipole-quadrupole, or quadrupole-quadrupole interaction, respectively. Γ is the gamma function: for $s=6$, $\Gamma\left(1-\frac{3}{s}\right) = 1.7725$ and for $s=8$, $\Gamma\left(1-\frac{3}{s}\right) = 1.4345$. Figure 4 shows the results of the simulation for $s=6$ and for $s=8$. The best fit is obtained with $s=6$, indicating that the dipole-dipole interaction is the main process responsible for the shortening of the fluorescence lifetime. The simulation yields a radiative lifetime $\tau_r = 61 \pm 1$ μs and a value of $\frac{N}{C_0} = 0.62 \pm 0.01$ for the critical ratio. From the $\frac{N}{C_0}$ value, a critical radius R_0 of 1.1 nm is retrieved. If we suppose a random distribution of Pr^{3+} ions, the fraction p of Pr^{3+} ions having at least one neighboring Pr^{3+} ion within the distance R_0 is given by[41]

$$p = 1 - e^{-N(4\pi/3)R_0^3}. \qquad (6)$$

From Eq. (6), 46% of the rare-earth ions have at least one Pr^{3+} ion within the distance R_0. This result confirms the validity of the Inokuti-Hirayama model to explain the fluorescence decay in 1.4% Pr^{3+}:$La_2(WO_4)_3$. Indeed, there is a high probability of finding one acceptor inside the critical radius of a donor, making the direct transfer process predominant and diffusion processes are thus not contributing to the energy-transfer mechanism. In order to evaluate the contribution of Γ_{pop} to Γ_h, we considered only the initial part of the decay curve ($t < 20$ μs) since the dephasing time evolves on a similar time scale. This initial part can be fitted by a single exponential corresponding to a lifetime of 11.5 μs, giving a contribution of 13.8 kHz to the homogeneous linewidth. From Eq. (6), it is also possible to determine the Pr concentration for which the direct relaxation process will be negligible. We consider that this direct process does not contribute to the lifetime if 1% or less ions have at least one neighboring Pr^{3+} ion within the distance R_0. A concentration of

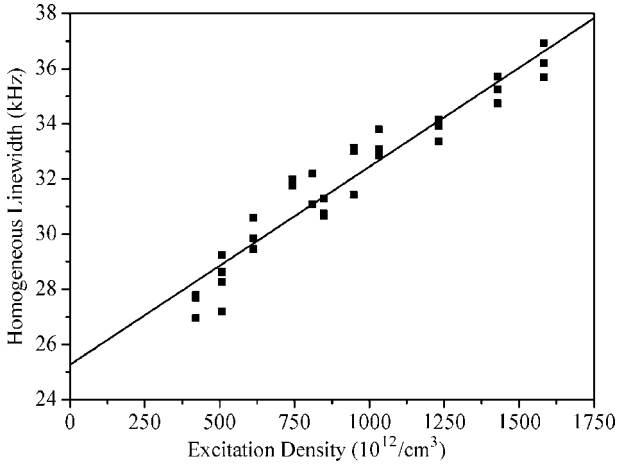

FIG. 5. Instantaneous spectral diffusion in the 1.4% Pr^{3+}:$La_2(WO_4)_3$ for the $^3H_4(0) \rightarrow {}^1D_2(0)$ transition.

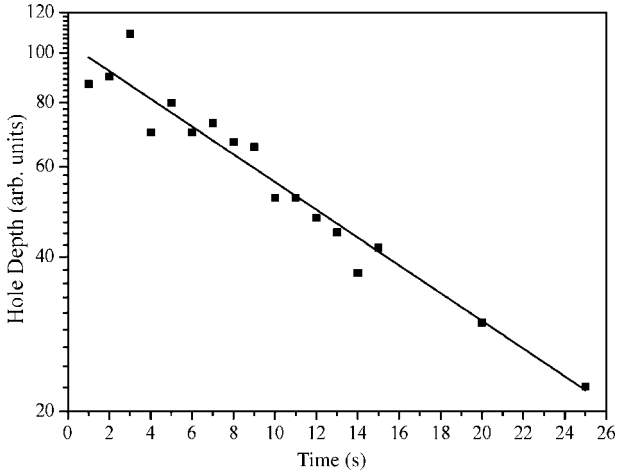

FIG. 6. Time decay of holes burnt in the $^3H_4(0) \rightarrow {}^1D_2(0)$ transition in 1.4% Pr^{3+}:$La_2(WO)_4$ compound. An exponential fit (solid line) gives a lifetime of 16±2 s.

around 2×10^{18} at./cm^3 is obtained, giving a doping level around 0.2%–0.3%. The ultimate limit on Γ_h is given by $\frac{1}{\pi(2\tau_r)}$, which yields a homogeneous linewidth of 2.6 kHz. This value is 2.5 times higher than the ultimate limit of site 1 in Y_2SiO_5: $T_1 = 164 \pm 5$ μs and $\Gamma_h(T_1) = 0.97$ kHz.[33]

The second term $\Gamma_{\text{ion-ion}}$ is due to excitation induced dephasing (instantaneous spectral diffusion). Excitation created by the echo sequence shifts the transition frequencies of neighboring ions and perturbs the phase relationships between the ions and thus reduces the echo intensity. This phenomenon is of interest for quantum gates in QC using REIC.[2] The $\Gamma_{\text{ion-ion}}$ term is strongly dependent on the concentration of the dopant and on the excitation intensity of the laser. In a crystal of fixed concentration, the $\Gamma_{\text{ion-ion}}$ contribution can be obtained by plotting Γ_h as a function of the excitation density ρ_{ex}. ρ_{ex} is given by $3 \times 10^{12} I \tau \alpha$ with τ the width of the excitation pulse in μs (0.5 μs in our experiments), I the laser intensity in W/cm^2, and α the absorption coefficient in cm^{-1}.[42] If we plot the measured Γ_h linewidth as a function of the excitation density (Fig. 5), the slope of the curve gives S_{ISD} which characterizes the instantaneous spectral diffusion (ISD) for a given material. We found a value of $S_{\text{ISD}} = 0.7 \times 10^{-11}$ Hz cm^3. As it is difficult to measure the absolute laser intensity, this value has a large uncertainty (around 30%). The broadening induced by the measurement itself is clearly seen on Fig. 5, and the extrapolation of the decay to zero excitation energy gives a homogeneous linewidth of 25.3±2.0 kHz. For Eu^{3+} and Pr^{3+} doped in Y_2SiO_5, $S_{\text{ISD}} = 0.9 \times 10^{-12}$ Hz cm^3 (Ref. 42) and $S_{\text{ISD}} = 1.2 \times 10^{-11}$ Hz cm^3 for site 1,[33] respectively. In Pr^{3+}:$La_2(WO_4)_3$, the instantaneous spectral diffusion is comparable to the one for site 1 in Pr^{3+}:Y_2SiO_5.

The third term $\Gamma_{\text{ion-spin}}$ is strongly dependent on the magnetic properties of the lattice. In principle, in the lanthanum compound, the high magnetic moment of La should have a significant contribution to the homogeneous linewidth. Impurities with electronic and nuclear moments can also contribute. From the fluorescence dynamics analysis of the $^1D_2$ level, we found $\Gamma_{\text{pop}} = 13.8$ kHz. Considering the extrapolated linewidth of 25.3 kHz at zero excitation energy, $\Gamma_{\text{ion-spin}}$ is estimated to be 25.3−13.8=11.5 kHz. This contribution can be reduced by decoupling the magnetic property of the lattice from the Pr^{3+} ions; this is why echo decays were also recorded in a static magnetic field of 14 mT to study the contribution from the magnetic fluctuations of the host crystal. Such low magnetic fields can have a significant effect on the coherence lifetime T_2 as demonstrated in Pr:YSO (Ref. 33) and in Pr:$KY(WO_4)_2$ (Ref. 43). However, no effect on the echo decay curve was measured in our case (Fig. 3). This suggests a high coupling between Pr^{3+} and the host nuclei La^{3+}.

C. Spectral-hole lifetime

The spectral-hole lifetime was measured by burning a hole at the center of the absorption line for 1 ms with a laser intensity of 15 W/cm.[2] The hole filling was measured for an observation period of 25 s (Fig. 6). The spectral-hole lifetime depends on the different spin-lattice relaxation rates among the three ground-state hyperfine levels. Several mechanisms including one-phonon processes, two-step Orbach processes, inelastic Raman scattering, and spectral diffusion through Pr-Pr interactions are possible.[42] By an exponential fit of the decay, a lifetime of 16±2 s was measured. This value characterizes the effective overall lifetime for the hole-burning process since different relaxation rates can occur between the different hyperfine splittings. The contribution of the one-phonon process is inefficient as the phonon density at the hyperfine frequency is very low. The contributions of the three other mechanisms were not analyzed on our work as we did not study the holes lifetime as a function of temperature and concentration.

IV. CONCLUSION

The hyperfine structure, the inhomogeneous and homogeneous linewidths, and the spectral-hole lifetime of the $^3H_4(0) \rightarrow {}^1D_2(0)$ transition in 1.4% Pr^{3+}:$La_2(WO_4)_3$ have been studied by photon-echo and spectral-hole-burning tech-

niques. The spectral diffusion brings an important contribution to the dephasing mechanisms of Pr^{3+} ions. Excited-state fluorescence decay measurements indicate a radiative lifetime of 61 ± 1 μs, giving a minimal homogeneous linewidth of 2.6 kHz. The inhomogeneous linewidth is 18.8 GHz for a 1.4% doping level and the effective hole lifetime is 16 ± 2 s.

By spectral-hole-burning spectroscopy, the hyperfine splittings of the ground $^3H_4(0)$ and excited $^1D_2(0)$ states were resolved and accurately studied. The spin-Hamiltonian hyperfine constants E and D were calculated.

The results obtained for the $La_2(WO_4)_3$ compound make this crystal an interesting host for quantum applications: (i) the peak absorption coefficient is 14.7 cm^{-1} with a low inhomogeneous linewidth, (ii) the hyperfine splittings are much higher than the homogeneous linewidth, and (iii) the hole lifetime is long enough to perform spectral selection. However, the dephasing time is too low for quantum information processing. Optimization of this material will include study of other Pr^{3+} concentrations, crystal growth conditions, and impurity identification.

ACKNOWLEDGMENTS

The authors would like to acknowledge financial support by the Access to Research Infrastructures activity in the 6th Framework programme of the EU (Contract No. RII3-CT-2003-506350, Laserlab Europe), the European Commission through the integrated project QAP and the Swedish Research Council. B.J. is supported by the Carlsberg Foundation.

*Author to whom correspondence should be addressed. Electronic address: olivier-guillotn@enscp.fr

[1] K. Ichimura, Opt. Commun. **196**, 119 (2001).
[2] N. Ohlsson, R. K. Mohan, and S. Kröll, Opt. Commun. **201**, 71 (2002).
[3] J. J. Longdell, E. Fraval, M. J. Sellars, and N. B. Manson, Phys. Rev. Lett. **95**, 063601 (2005).
[4] M. Nilsson and S. Kröll, Opt. Commun. **247**, 393 (2005).
[5] J. J. Longdell, A. L. Alexander, and M. J. Sellars, Phys. Rev. B **74**, 195101 (2006).
[6] R. M. Macfarlane, J. Lumin. **100**, 1 (2002).
[7] J. I. Cirac, P. Zoller, H. J. Kimble, and H. Mabuchi, Phys. Rev. Lett. **78**, 3221 (1997).
[8] A. E. Kozhekin, K. Mölmer, and E. Polzik, Phys. Rev. A **62**, 033809 (2000).
[9] S. A. Moiseev and S. Kröll, Phys. Rev. Lett. **87**, 173601 (2001).
[10] M. Fleischhauer and M. D. Lukin, Phys. Rev. A **65**, 022314 (2002).
[11] D. F. Phillips, A. Fleischhauer, A. Mair, R. L. Walsworth, and M. D. Lukin, Phys. Rev. Lett. **86**, 783 (2001).
[12] B. Julsgaard, J. Sherson, J. I. Cirac, J. Fiurasek, and E. Polzik, Nature (London) **432**, 482 (2004).
[13] T. Chanelière, D. N. Matsukevich, S. D. Jenkins, S. Y. Lan, T. A. B. Kennedy, and A. Kuzmich, Nature (London) **438**, 833 (2005).
[14] M. D. Eisaman, A. André, F. Massou, M. Fleischhauer, A. S. Zibrov, and M. D. Lukin, Nature (London) **438**, 837 (2005).
[15] B. Kraus, W. Tittel, N. Gisin, M. Nilsson, S. Kröll, and J. I. Cirac, Phys. Rev. A **73**, 020302(R) (2006).
[16] A. L. Alexander, J. J. Longdell, M. J. Sellars, and N. B. Manson, Phys. Rev. Lett. **96**, 043602 (2006).
[17] M. Nilsson, Ph.D. thesis, Lund Institute of Technology, 2004.
[18] R. M. Macfarlane and R. M. Shelby, in *Spectroscopy of Solids Containing Rare Earth Ions*, edited by A. A. Kaplyanskii and R. M. Macfarlane (North-Holland, Amsterdam, 1987), p. 51.
[19] A. Caprez, P. Meyer, P. Mikhail, and J. Hulliger, Mater. Res. Bull. **32**, 1045 (1997).
[20] Ph. Goldner and O. Guillot-Noël, Mol. Phys. **102**, 1185 (2004).
[21] O. Guillot-Noël, Ph. Goldner, E. Antic-Fidancev, and J. L. Le Gouët, Phys. Rev. B **71**, 174409 (2005).
[22] F. de Seze, A. Louchet, V. Crozatier, I. Lorgeré, F. Bretenaker, J. L. Le Gouët, O. Guillot-Noël, and Ph. Goldner, Phys. Rev. B **73**, 085112 (2006).
[23] M. Nilsson, L. Rippe, N. Ohlsson, T. Christiansson, and S. Kröll, Phys. Scr., T **T102**, 178 (2002).
[24] M. Nilsson, L. Rippe, S. Kröll, R. Klieber, and D. Suter, Phys. Rev. B **70**, 214116 (2004).
[25] L. Rippe, M. Nilsson, S. Kröll, R. Klieber, and D. Suter, Phys. Rev. A **71**, 062328 (2005).
[26] J. J. Longdell, M. J. Sellars, and N. B. Manson, Phys. Rev. Lett. **93**, 130503 (2004).
[27] R. D. Shannon and G. T. Prewitt, Acta Crystallogr., Sect. B: Struct. Crystallogr. Cryst. Chem. **B25**, 925 (1969).
[28] X. Lin, Y. Chen, J. Liao, Z. Luo, and Y. Huang, J. Cryst. Growth **266**, 487 (2004).
[29] M. Gaertner, D. Abeln, A. Pring, M. Wilde, and A. Reller, J. Solid State Chem. **111**, 128 (1994).
[30] M. A. Teplov, Sov. Phys. JETP **26**, 872 (1968).
[31] J. J. Longdell, M. J. Sellars, and N. B. Manson, Phys. Rev. B **66**, 035101 (2002).
[32] K. Holliday, M. Croci, E. Vauthey, and U. P. Wild, Phys. Rev. B **47**, 14741 (1993).
[33] R. W. Equall, R. L. Cone, and R. M. Macfarlane, Phys. Rev. B **52**, 3963 (1995).
[34] M. J. Sellars, E. Fraval, and J. J. Longdell, J. Lumin. **107**, 150 (2004).
[35] M. J. Weber, Phys. Rev. B **4**, 2932 (1971).
[36] A. Lorenzo, L. E. Bausa, and J. Garcia Solé, Phys. Rev. B **51**, 16643 (1995).
[37] A. O. Wright, M. D. Seltzer, J. B. Gruber, B. Zandi, L. D. Merkle, and B. H. T. Chai, J. Phys. Chem. Solids **57**, 1337 (1996).
[38] B. Savoini, J. E. Munoz Santiuste, and R. Gonzalez, Phys. Rev. B **56**, 5856 (1997).
[39] R. Balda, J. Fernandez, I. S. de Ocariz, M. Voda, A. J. Garcia, and N. Khaidukov, Phys. Rev. B **59**, 9972 (1999).
[40] M. Inokuti and F. Hirayama, J. Chem. Phys. **43**, 1978 (1965).
[41] R. S. Quimby, W. J. Miniscalco, and B. Thompson J. Appl. Phys. **76**, 4472 (1994).
[42] F. Könz, Y. Sun, C. W. Thiel, R. L. Cone, R. W. Equall, R. L. Hutcheson, and R. M. Macfarlane, Phys. Rev. B **68**, 085109 (2003).
[43] H. L. Xu, M. Nilsson, S. Ohser, N. Rauhut, S. Kröll, M. Aguilo, and F. Diaz, Phys. Rev. B **70**, 214115 (2004).